ELSEVIER

Coastal Engineering 33 (1998) 155–176

COASTAL ENGINEERING

Surf zone dynamics simulated by a Boussinesq type model. III. Wave-induced horizontal nearshore circulations

O.R. Sørensen *, H.A. Schäffer, P.A. Madsen

International Research Centre for Computational Hydrodynamics (ICCH), Danish Hydraulic Institute, Agern Alle 5, 2970 Hørsholm, Denmark

Received 25 June 1997; revised 30 December 1997; accepted 12 January 1998

Abstract

This is the third of three papers on the modelling of various types of surf zone phenomena by the use of a time-domain Boussinesq type model, which is extended to the surf zone and swash zone by including a simple description of wave breaking and a moving boundary at the shoreline. In the first paper [Madsen, P.A., Sørensen, O.R., Schäffer, H.A., 1997. Surf zone dynamics simulated by a Boussinesq type model: Part 1. Model description and cross-shore motion of regular waves. Coastal Eng. 32, 255–288.], the numerical model was described and it was applied to study cross-shore motion of regular waves in the surf zone including shoaling, breaking and runup. The first paper also included a discussion of time-averaged quantities derived from the time-domain solutions. The second paper [Madsen, P.A., Sørensen, O.R., Schäffer, H.A., 1997. Surf zone dynamics simulated by a Boussinesq type model: Part 2. Surf beat and swash oscillations for wave groups and irregular waves. Coastal Eng. 32, 289–320.] treated the cross-shore motion of wave groups and irregular waves with emphasis on the resulting shoreline motion and surf beat. The present paper concentrates on wave breaking and wave-induced currents in the horizontal plane. This is done without the traditional splitting of the phenomenon into a wave problem and a current problem. Mutual interaction between short waves and long waves and wave-induced (depth-averaged) currents is inherent in the model. Two situations are studied with waves normally incident on a plane sloping beach, but with some alongshore non-uniformity. In the first example, a rip channel is present and the other concerns a detached breakwater parallel to the shoreline. In both situations, wave-driven currents are generated and circulation cells appear. In turn, the currents appear to affect the waves. Results are presented for the case of unidirectional

* Corresponding author.

PII S0378-3839(98)00007-6

waves as well as for directionally spread waves. The resulting current patterns and wave height distributions are shown to be in good agreement with laboratory measurements from the literature.

Keywords: Surf zone; Boussinesq model; Wave breaking; Wave-induced currents; Horizontal nearshore circulation; Rip channel; Detached breakwater

1. Introduction

The classical procedure for describing wave-driven depth-averaged currents is based on a decoupled approach. First, the wave field is determined by linear wave theory where the energy dissipation is modelled by empirical relations and then the currents are determined by solving the depth-integrated flow equations including radiation stresses, bottom friction and viscosity. The first premature models of nearshore currents, which appeared in the early seventies, neglected many of the important effects such as convection and viscosity in the flow equations, and more detailed models were reported by, e.g., Ebersole and Dalrymple (1979), Vreugdenhil (1980) and Wu and Liu (1982). The wave fields were, however, at that time determined by relatively simple means limited to refraction of unidirectional linear monochromatic waves. Reviews of the state-of-the-art surf zone models of those days can be found in Basco (1982, 1983).

In the years to follow, the decoupled approach was refined by introducing more and more sophisticated but still linear wave models, including, e.g., diffraction and breaking criteria for random waves while current refraction was incorporated by successive and iterative executions of the flow models and wave models. A review focusing on wave-induced nearshore circulations was given by Battjes et al. (1990) and one of their conclusions was that although the decoupled concept of wave-flow modelling in the surf zone had reached a more mature state, only steady circulations could be determined, while no models could yet handle low-frequency motions in the surf zone.

Seven years earlier, Basco (1983) had already foreseen that Boussinesq theory could offer the possibility to raise the fundamental knowledge of coastal hydrodynamics to a higher level, since this type of equations had the potential to describe not only the primary wave motion, but also the currents they induce as well as the interaction between the two. This statement was criticised by Kirby and Dalrymple (1984) who believed that with regard to the wave-induced currents Boussinesq-type theory could only provide the primary-wave forcing to be used for a decoupled current calculation. Time has shown that Basco was correct in the sense that a time domain Boussinesq model would automatically include the combined effects of wave–wave and wave–current interaction in shallow water without the need for successive wave-model and flow-model executions, without the need for explicit formulations of the radiation stress, and with the potential of being the tool for investigating interaction between wave groups and low-frequency motions. However, by that time, the main problem was the incorporation of wave breaking.

Early attempts of incorporating wave breaking in one-dimensional Boussinesq models were made by, e.g., Abbott et al. (1983), Deigaard (1989) and Karambas et al. (1990), and a review of these models can be found in Schäffer et al. (1993) and Madsen et al.

(1997a). The first examples of two-dimensional Boussinesq type surf zone models were presented only recently by Prüser (1991), Schäffer et al. (1992), Kabiling and Sato (1993) and Sørensen et al. (1994).

The Boussinesq models of Prüser (1991) and Kabiling and Sato (1993) have several similarities: In both cases, wave breaking is taken into account by adding eddy viscosity terms to the momentum equations, and the breaking criterion is based on the local ratio, α, of the wave particle velocity to the wave celerity. In both cases, the critical value of α is established empirically as a function of the incident wave steepness. Calibrated values of α were found to be from 0.78 to 0.9 by Prüser and from 0.5 to 0.75 by Kabiling and Sato. Prüser approximates the wave celerity by the speed of the corresponding solitary wave, a method which is likely to overestimate the wave celerity and which is not influenced by the presence of long waves or currents; Kabiling and Sato estimate the wave celerity from the gradient of the phase lag by involving Fourier analysis of the computed surface elevation, a method which is not straightforward to apply in connection with time-domain modelling of spatially varying wave trains. Finally, Prüser establishes the viscosity due to wave breaking as a function of wave steepness and bed slope, while Kabiling and Sato use an expression proposed by Watanabe and Dibajnia (1988).

Major drawbacks in the procedures suggested by Prüser and by Kabiling and Sato are as follows. Firstly, the breaker models are not genuine time-domain models but rather an attempt to transfer empirical frequency domain criteria to the time domain. For the same reason, it is not obvious to which extent the models can be applied to the case of wave groups and irregular waves and to the case of waves in ambient currents. Secondly, dissipation is introduced by viscosity terms based on spatial gradients of velocity. Such terms are known to smear out the effects of breaking without being able to retain basic physical phenomena such as the pronounced vertical asymmetry in breaking waves.

The present work represents an extension of Schäffer et al. (1992, 1993), Madsen et al. (1994) and Sørensen et al. (1994). As explained in Part I of this work (Madsen et al., 1997a), wave breaking is based on the surface roller concept for spilling breakers using a geometrical determination of the instantaneous roller thickness at each point and modelling the effect of wave breaking by additional convective momentum terms. These are functions of the local wave celerity components. The moving shoreline is treated numerically by replacing the solid beach by a permeable beach characterized by an extremely small porosity. The model is based on the Boussinesq equations derived by Madsen et al. (1991) and Madsen and Sørensen (1992). These equations reproduce the feature of wave–current interaction, but are only accurate for the case of weak currents, since the Doppler shift is not correctly represented. A correct form of the Doppler shift requires additional nonlinear terms, as first derived by Yoon and Liu (1989). Boussinesq-type equations valid for stronger currents and larger dispersion can be found in Madsen and Schäffer (1998) and Chen et al. (1996).

This paper is organized as follows. Special details of the breaker model relevant for two-dimensional surf zone calculations are given in Section 2, which contains a description of numerical details, the 2D-detection of surface rollers and the formulation of bottom friction. Section 3 presents model results for two cases of wave-induced circulations. One example concerns a beach with a rip channel subject to monochromatic

incident waves. The other example is a beach with a detached breakwater, where both regular, unidirectional waves and irregular, directionally spread waves are studied. Comparison is made with laboratory data by Hamm (1992a) and Mory and Hamm (1997).

2. Model details relevant for 2D-horizontal cases

Although the model was presented in Part I of this work, some specific issues need to be addressed in the two-dimensional applications: Numerical aspects need special attention; the determination of the surface roller is somewhat more complicated than in the one-dimensional case and bottom friction can no longer be ignored.

2.1. Numerical aspects

The differential equations are discretized using a time-centered implicit scheme with variables defined on a space-staggered rectangular grid. The method is based on the Alternating Direction Implicit algorithm. For more details of the solution procedure reference is made to Madsen et al. (1991) and Madsen and Sørensen (1992). The finite-difference approximation of the spatial derivatives is generally a straightforward mid-centering. However, in the present work, we have treated the nonlinear convective terms somewhat differently. The use of high-order central schemes for the discretization of convective terms is known to introduce nonphysical oscillations in regions with large gradients of the convected variables. Typically, these appear around corners of structures, e.g., at the tip of a breakwater, in regions of strong wave-induced circulations, and in the bore-like stage in the inner surf zone.

A large number of oscillation-free schemes have been proposed in the literature, especially within the field of compressible flows with strong shocks (see, e.g., LeVeque (1990) and Vreugdenhil and Koren (1993)). To avoid artificial damping of the wave motion, it is essential to maintain high accuracy in smooth regions of the flow and only increase the amount of numerical diffusion in regions with steep gradients in the flow variables. One approach is to apply a high order method and add artificial viscosity terms. The main problem with this approach is the quantification of the viscosity to avoid the oscillations without causing unnecessary smearing. Kabiling and Sato (1993) applied the artificial viscosity approach for simulation of waves propagating on a plane sloping beach with a detached breakwater. However, the viscosity was not determined based on local flow condition, but was a function of the distance from the shoreline and the local bed slope. In the present work, a different method is applied based on a simple hybridization of a high order and a low order scheme. A second-order (quadratic) upwinding scheme is used in areas where the solution is smooth, while a first-order upwinding (simple) scheme is used in sharply varying areas. The switch to simple upwinding is done, when the absolute value of the second-difference of the local depth-integrated velocity is larger than the absolute value of the first-difference of the local depth-integrated velocity. This criterion was suggested by Leonard (1991).

2.2. Determination of surface rollers

The determination of the surface roller is described in this section, beginning with a summary of the case of only one horizontal dimension as treated in Part I.

Breaking is assumed to start when and where the local steepness of the wave front exceeds a certain limiting gradient $\tan\phi$. The toe of the roller is defined as the location where the wave steepness is identical to $\tan\phi$, and we approximate the geometry of the roller by using the tangent of slope $\tan\phi$, starting at the toe and pointing in the direction opposite to the direction of wave propagation. The thickness of the roller, δ is determined simply as the water above this tangent, but multiplied by a shape factor f_δ prior to inclusion in the governing equations.

To account for the transition from the initial breaking to the bore-like stage in the inner surf zone, the critical roller angle, ϕ, is assumed to vary as the function of the age of each surface roller: ϕ is initiated to ϕ_B, and from the time of incipient breaking, t_B, it is assumed to decrease according to:

$$\tan\phi(t) = \tan\phi_0 + (\tan\phi_B - \tan\phi_0)\exp\left[-\ln 2\frac{t-t_B}{t_{1/2}}\right], \tag{2.1}$$

where ϕ_0 is the terminal value of $\phi(t)$ and $t_{1/2}$ is the half time for the transition. The following values were used in all the results presented below: $\phi_B = 20°$, $\phi_0 = 10°$ and $t_{1/2} = T/5$ where T is a typical period of the waves. For the shape factor, a value of $f_\delta = 1.5$ was used. These parameter values are identical to the default parameter set used in Parts I and II (Madsen et al. (1997a,b)).

In the two horizontal dimensions, the toe of the roller becomes a curve instead of a single point and the tangent becomes a tangential surface separating the roller from the rest of the flow (see Fig. 1a). The roller toe curve is defined as the points satisfying the condition that the absolute value of the gradient equals the instantaneous local value of $\tan\phi$ and that the gradient in the direction of the wave propagation is negative. In the

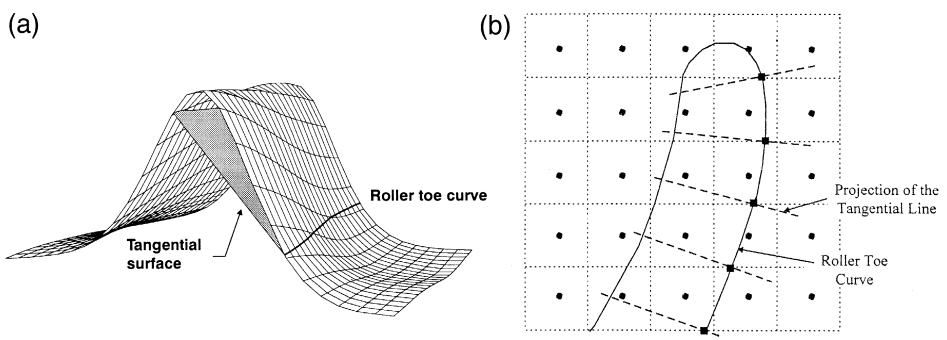

Fig. 1. Illustration sketch for determination of the surface roller. (a) Instantaneous surface elevation of a breaking wave and (b) horizontal plane. ●, Surface elevation and gradient points; and ■, Toe points of the roller.

two-dimensional case, the roller angle $\phi(t)$ is allowed to vary within a roller because different stages of the breaking process can be represented within the same roller. For example, when oblique regular waves break on a beach with straight and parallel depth contours, both the initial and the final stages of the breaking process may be represented within the same roller. Hence, it is necessary to keep track of the surface roller age along the orthogonal to the roller toe curve.

The surface roller detection appears quite simple in a continuous description, but it becomes more complicated in the required discrete formulation. A discrete representation of the spatial variation of the roller thickness, wave celerity and roller angle is introduced. First, the discrete toe points of the rollers and the tangential lines at these points are determined. Let a rectangular grid be defined by having a surface elevation node in the center of each grid cell (see Fig. 1b). Centered values of the roller angle and the surface elevation gradient are then calculated at the nodes of this grid and subgrid roller toe points satisfying the toe condition are found by interpolation at the boundary of each cell. The surface elevation and the direction of wave propagation are computed at the roller toe points. The roller toe is assumed to vary linearly between each pair of roller toe points. Next, the roller thickness is determined. In each element with two toe points, the tangential lines at the toe points constitute the tangential surface. Sweeping through the area enclosed between the roller toe curve and the projection on the horizontal plane of the two tangential lines, we determine the roller thickness. The sweep in terminated when the back of the roller is reached. Finally, the roller angle is updated. Between each pair of generating lines used for the roller determination and in the near vicinity of the roller toe curve, $\phi(t)$ decays according to Eq. (2.1).

The roller celerity is computed by using:

$$\begin{pmatrix} c_x \\ c_y \end{pmatrix} = \begin{pmatrix} \dfrac{\partial \eta}{\partial x} \\ \dfrac{\partial \eta}{\partial y} \end{pmatrix} \frac{1.3\sqrt{gh}}{\sqrt{\left(\dfrac{\partial \eta}{\partial x}\right)^2 + \left(\dfrac{\partial \eta}{\partial y}\right)^2}}, \tag{2.2}$$

where η is the surface elevation, h is the still water depth and (x, y) are the Cartesian coordinates. The derivatives are evaluated at the roller toe. This is a directional version of $c = 1.3\sqrt{gh}$, which was discussed in Section 2.4 of Part I. Although this approximation was shown to give good results for regular waves, it clearly does not capture features like the deceleration of primary waves due to downrush of long waves in the swash zone. Such phenomena, which can be important for irregular waves, call for an interactively determined celerity as used in Parts I and II, but not yet implemented in two horizontal dimensions.

2.3. Bottom friction and mixing processes

As opposed to the shore-normal case, steady solutions for the mean flow can only exist when the forcing by radiation stress is balanced by bottom friction and mixing

processes. Mixing processes are usually modelled by means of an eddy viscosity. In the breaking zone, the viscous shear is to some extent taken into account by the additional convective terms due to the roller. Outside the breaking zone, the eddy viscosity is

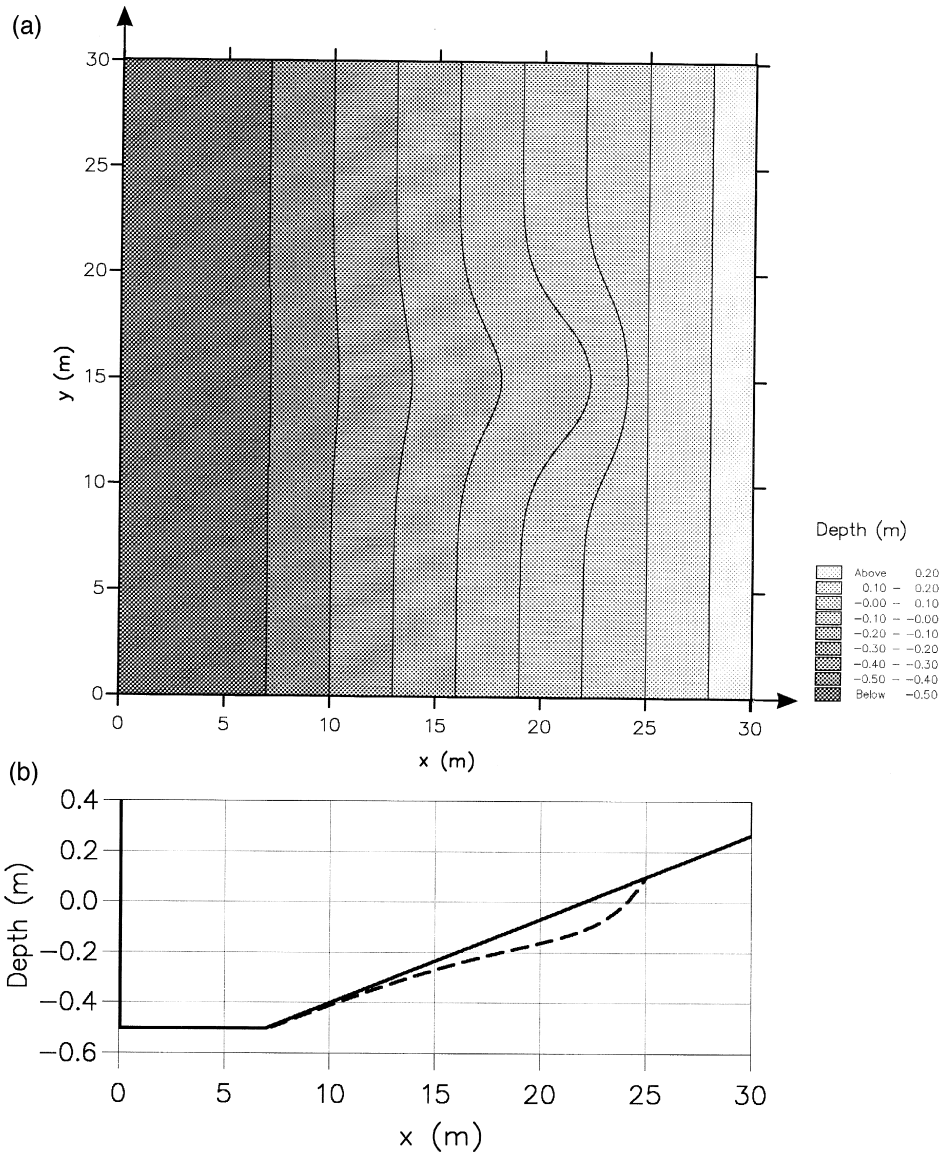

Fig. 2. Model setup for the rip channel test. (a) Contour plot of the bathymetry and (b) beach profiles. ————, Along a plane beach section; and ---, Along the rip channel.

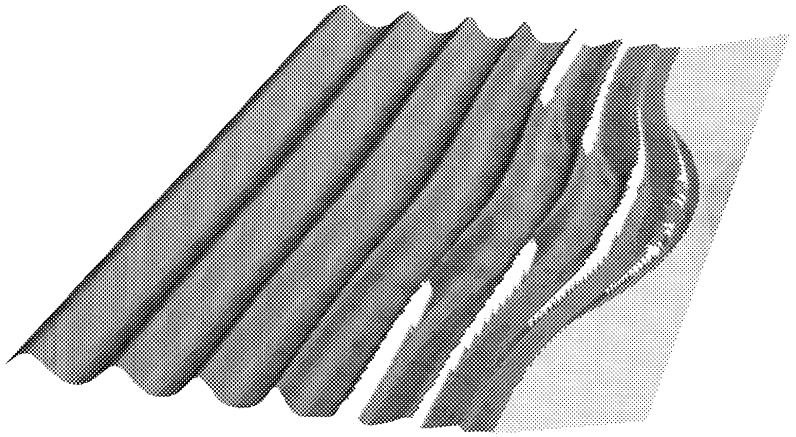

Fig. 3. Instantaneous surface elevation for the rip channel case (the surface rollers are shown in white) before the circulation cell has developed.

usually found to be very small and therefore no eddy viscosity terms are included in the simulations. In the present computations, the bottom shear stress is modelled using:

$$(\tau_x,\tau_y) = \frac{1}{2} f_{\mathrm{m}}\, \rho \frac{\sqrt{P^2+Q^2}}{d^2}(P,Q), \tag{2.3}$$

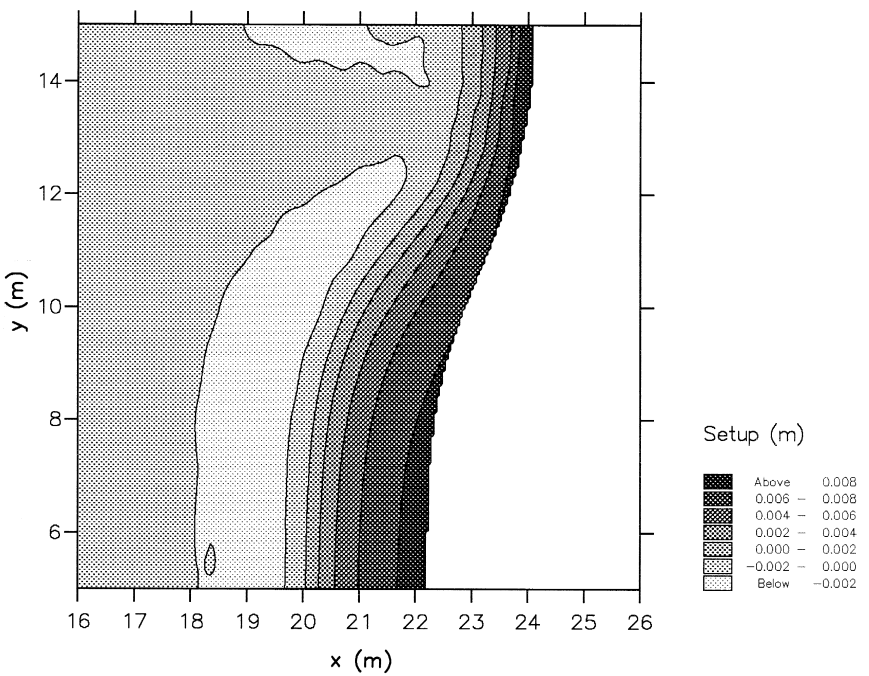

Fig. 4. Contour plot of the computed setup.

where f_m is the friction factor, (P,Q) are the depth-integrated velocities (the volume fluxes) in the Cartesian coordinate system and d is the instantaneous depth. This simple formulation does not represent the effect of turbulent interaction between oscillatory boundary layers and the mean flow.

3. Waves and wave-induced currents on beaches

We have chosen two situations with waves normally incident on a plane sloping beach but with some alongshore non-uniformity to trigger nearshore circulation. In the first example, a rip channel is present while the other example concerns a detached breakwater parallel to the shoreline. Laboratory experiments are available for both cases. While the experimental data on the rip current test are rather sparse, the extensive measurements for the detached breakwater case provide an excellent test for the numerical model.

3.1. A rip channel

The first example is chosen according to laboratory experiments reported by Hamm (1992a,b). The wave basin is 30 m × 30 m and the bathymetry is a plane sloping beach of 1:30 with a rip channel excavated along the centerline. The bathymetry is shown in Fig. 2. Hamm considered a number of different incident wave conditions of which we

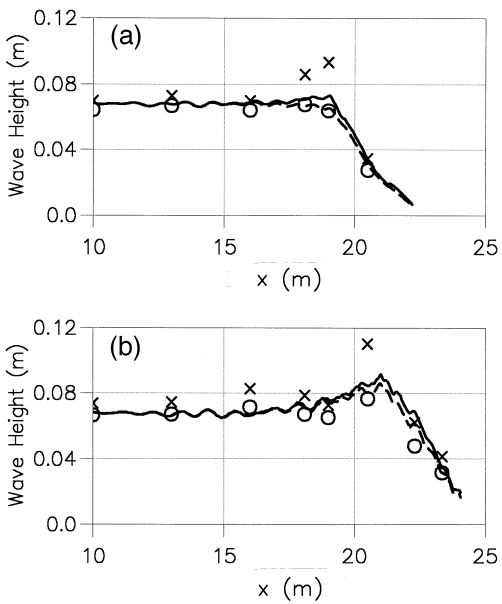

Fig. 5. Comparison between the computed and measured cross-shore variation of the wave height. (a) Along a plane beach section and (b) along the rip channel. ————, Mean wave height, H_m—present model; ---, Variance-based wave height, $H_\sigma/\sqrt{2}$—present model; x, Significant wave height, $H_{1/3}$—experimental data by Hamm (1992b); o, Variance-based wave height, $H_\sigma/\sqrt{2}$—experimental data by Hamm (1992b).

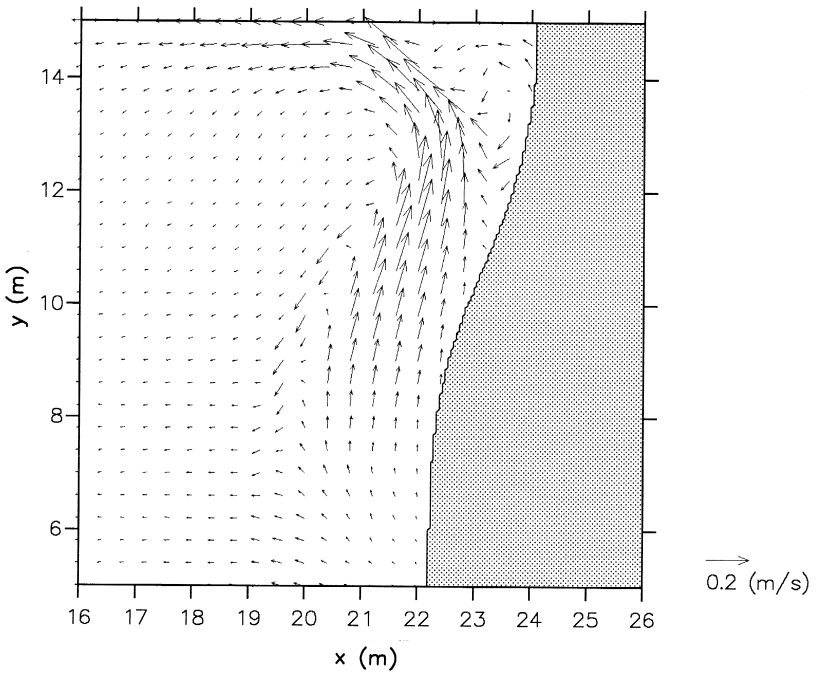

Fig. 6. Depth-averaged velocity focusing on a circulation cell. The centerline of the rip channel is at the top ($y = 15$ m) and the shoreline is to the right.

shall concentrate on one: unidirectional, regular, incident waves with a period of 1.25 s and a wave height of 0.07 m at the offshore boundary.

Using a reflective boundary condition at the line of symmetry, i.e., at the centerline of the rip channel, only half of the physical wave tank was covered in the numerical computations. The grid spacing was 0.05 m, the time step 0.02 s and the simulation

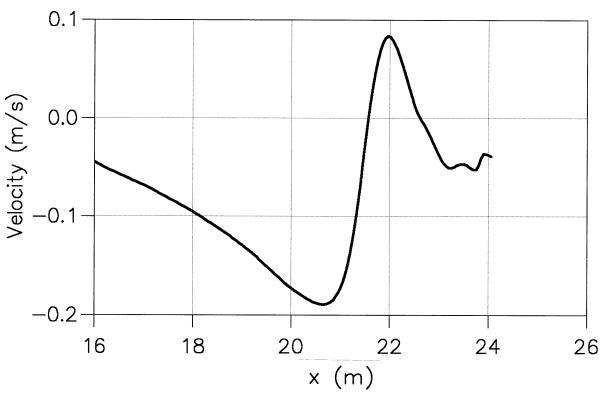

Fig. 7. Rip current along the rip channel.

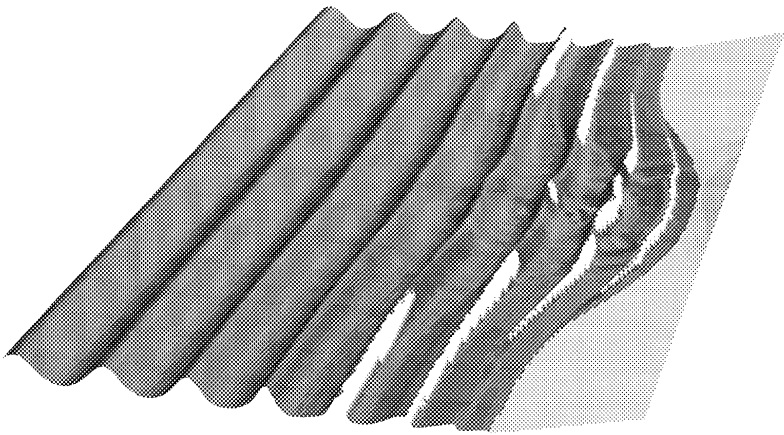

Fig. 8. Instantaneous surface elevation for the rip channel case at a time when the circulation cell has fully developed.

period was 600 s corresponding to 480 wave periods. A constant friction factor of $f_m = 0.03$ was used in the bed friction term. This value was determined by calibration.

The wave field in a subdomain is shown in Fig. 3. This picture is taken just after the simulation is started ($t = 40$ s). The surface rollers are shown in white. Due to the increased depth and due to depth refraction by the rip channel, incipient breaking is seen to occur comparatively close to the shore along the centerline. Here, the setup is quite small and the larger setup appearing away from the rip channel gives an alongshore

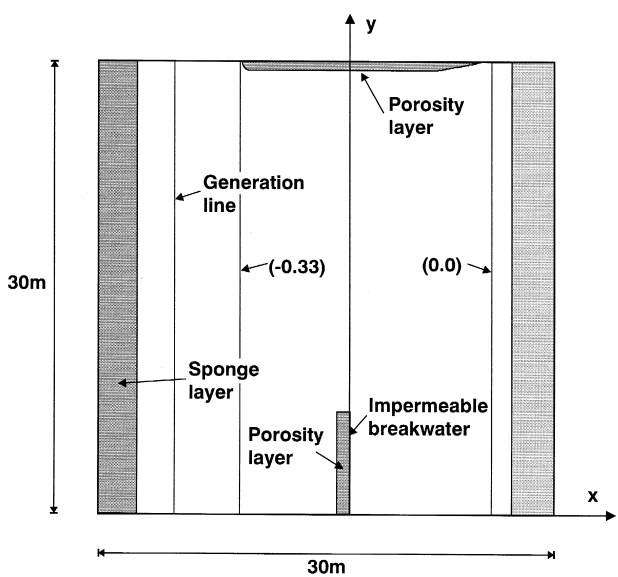

Fig. 9. Model setup for the detached breakwater test.

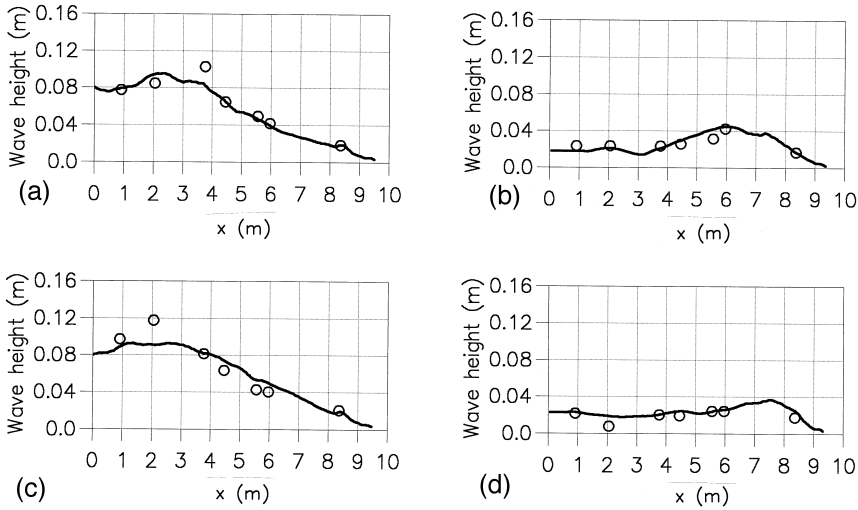

Fig. 10. Cross-shore variation of the mean wave height, H_m, for the case of regular unidirectional waves. (a) $y = 16$ m, (b) $y = 9$ m, (c) $y = 5$ m and (d) $y = 1$ m. ————, Present model; o, Experimental data by Hamm et al. (1995).

gradient in the mean water surface forcing a current towards the centerline. The flow from the two sides join to form a rip current and two symmetrical circulation cells appear. A steady state wave-induced current field is reached after approximately 120 wave periods (150 s). A contour plot of the setup is shown in Fig. 4. Fig. 5a shows the

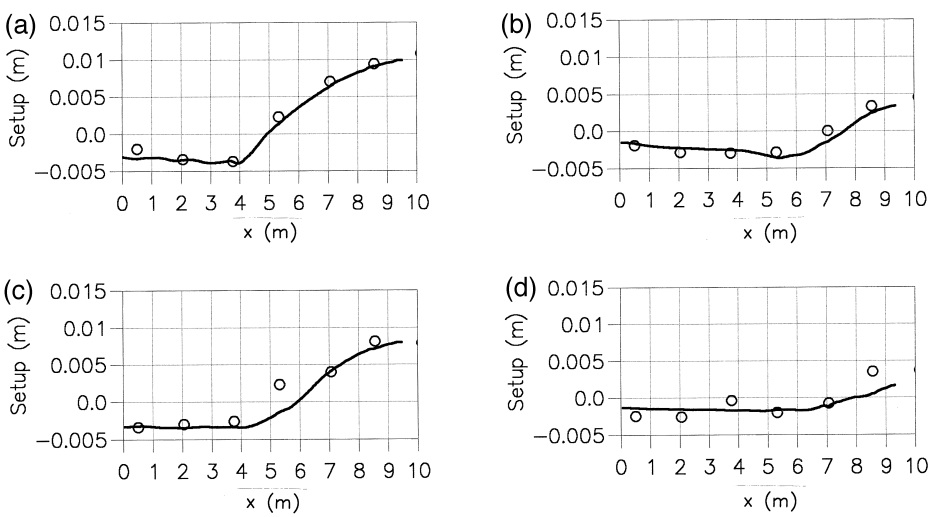

Fig. 11. Cross-shore variation of the setup for case of regular unidirectional waves. (a) $y = 16$ m, (b) $y = 9.39$ m, (c) $y = 6.29$ m and (d) $y = 3.19$ m. ————, Present model; o, Experimental data by Hamm et al. (1995).

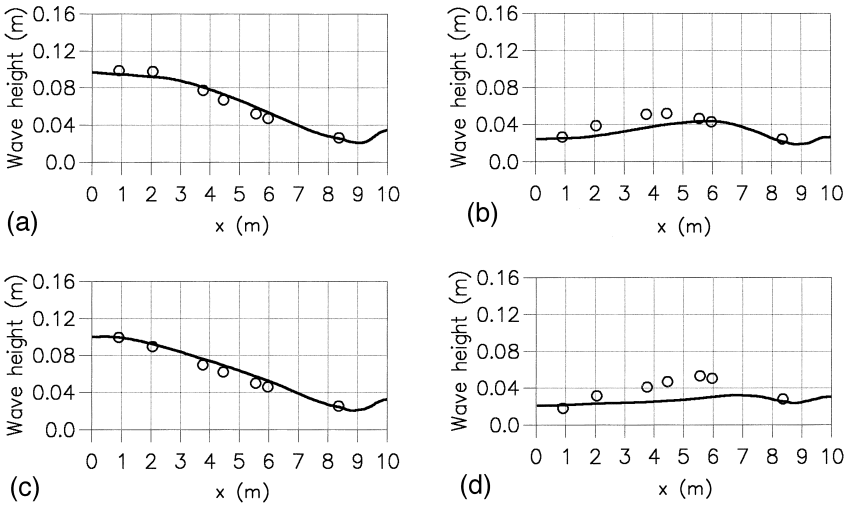

Fig. 12. Cross-shore variation of the energy based wave height, H_{m0} for the case of irregular multidirectional waves. (a) $y = 16$ m, (b) $y = 9$ m, (c) $y = 5$ m and (d) $y = 1$ m. ————, Present model; o, Experimental data by Hamm et al. (1995).

cross-shore variation of the wave height at some distance from the rip channel where the beach is a plane slope. A similar plot, but along the excavated beach at the centerline, is shown in Fig. 5b. The measurements of Hamm are included for comparison and the agreement is quite good.

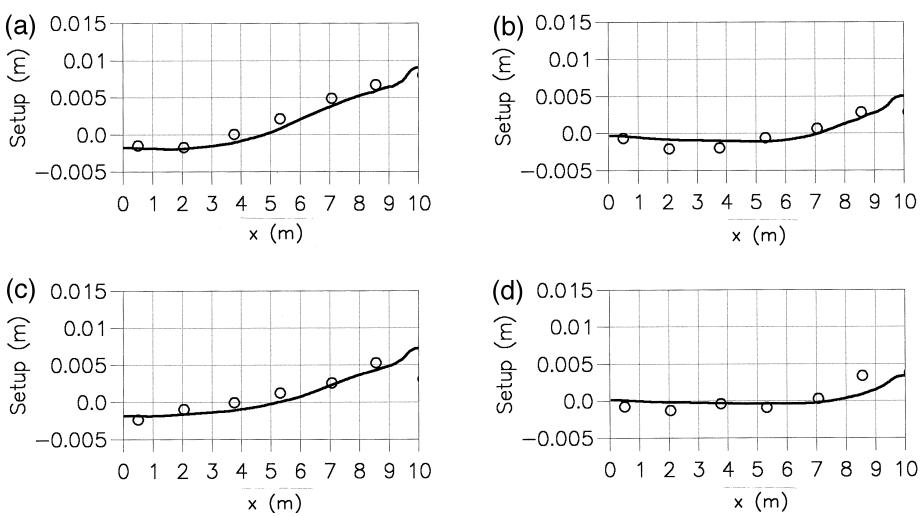

Fig. 13. Cross-shore variation of the setup for case of irregular multidirectional waves. (a) $x = 16$ m, (b) $y = 9.39$ m, (c) $y = 6.29$ m and (d) $y = 3.19$ m. ————, Present model; o, Experimental data by Hamm et al. (1995).

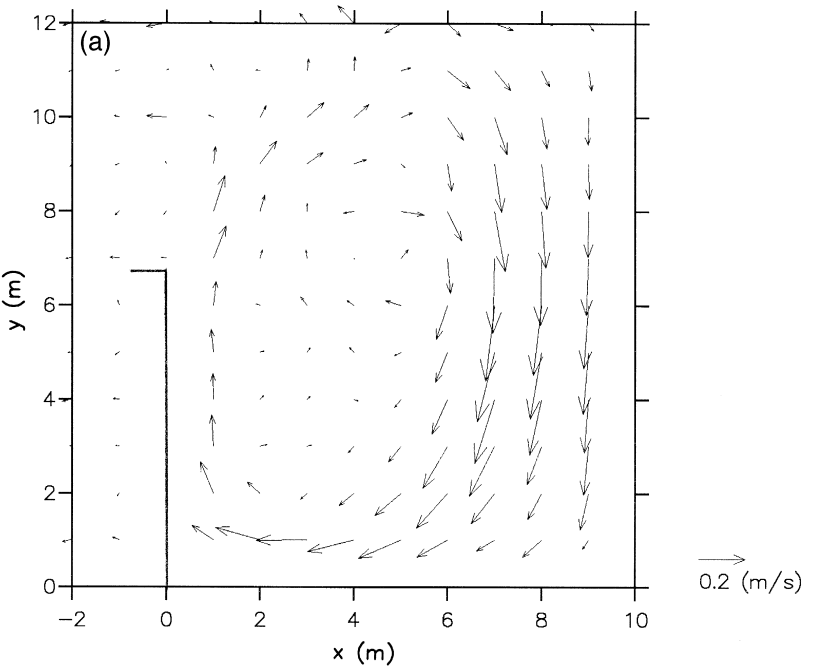
(a)
y (m)
x (m)
0.2 (m/s)

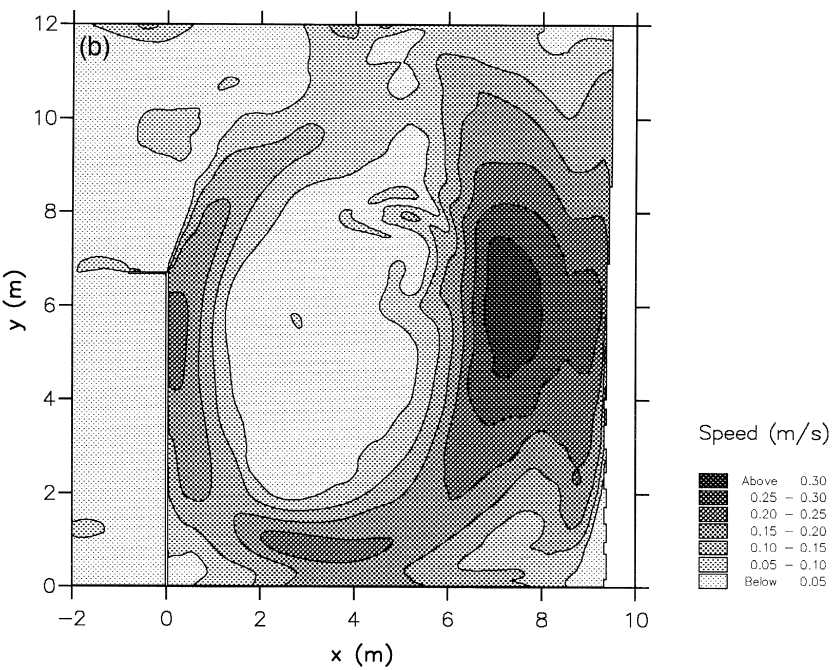
(b)
y (m)
x (m)
Speed (m/s)
Above 0.30
0.25 – 0.30
0.20 – 0.25
0.15 – 0.20
0.10 – 0.15
0.05 – 0.10
Below 0.05

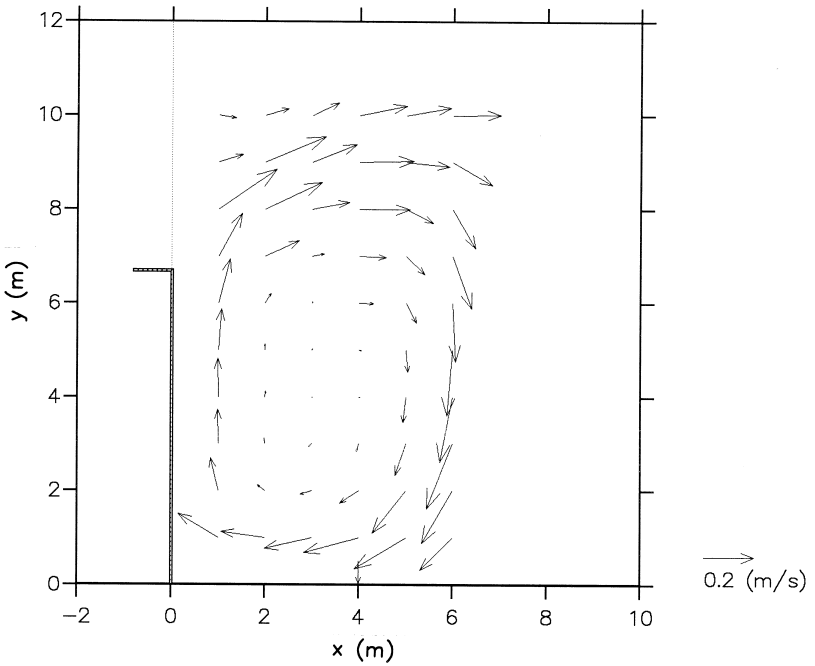

Fig. 15. Circulation cell behind the detached breakwater for the case of regular, unidirectional waves. Measured time-average of the horizontal velocities at mid-depth (Hamm et al., 1995).

A vector plot of the steady state velocity field is shown in Fig. 6. The velocity is computed as the time-average of the depth-averaged velocity below the roller, u_0. It should be noted that vectors are shown only at every 8 grid points. A subdomain is shown in order to focus on the circulation cells which have developed. A pronounced rip current is seen along the centerline of the bathymetry, i.e., at the top of the figure. Fig. 7 shows the cross-shore variation of the rip current. For reasons of symmetry, the rip current was bound to be directed exactly perpendicular to the shore. In Hamm's experiments, the measured rip current showed a significant deviation from this direction. In principle, this could be due to instabilities of the rip current. However, the explanation is more likely to be imperfections in the supposedly symmetrical experiment. (The detailed report on the experiments (Hamm, 1992b) shows results for the same test, but without the rip channel, i.e., uniform conditions in the alongshore direction. Even in this case lateral differences in wave height and nearshore setup exceeded 10 and 20%, respectively.) In the experiment, a maximum of 0.25 m/s for the mean return current near the bottom was measured indicating that with regard to the order of magnitude of the rip current speed, the numerical simulation agrees with the experimental results. The

Fig. 14. Circulation cell behind the detached breakwater for the case of regular, unidirectional waves. Computed time-average of the velocities beneath the surface rollers. (a) Vector plot and (b) contour plot of the speed.

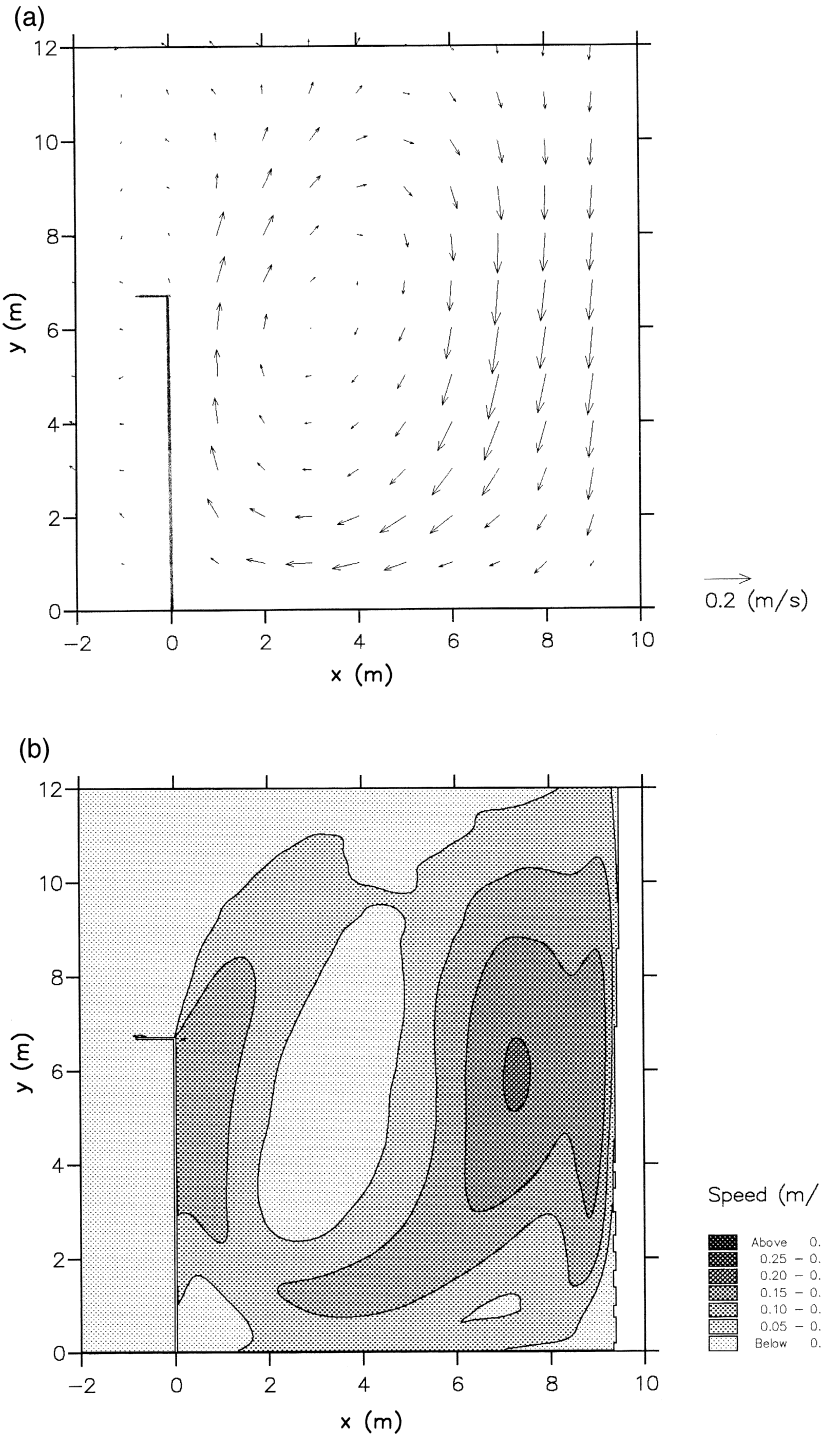
(a)
y (m)
x (m)
0.2 (m/s)
(b)
y (m)
x (m)
Speed (m/s)
Above 0.30
0.25 – 0.30
0.20 – 0.25
0.15 – 0.20
0.10 – 0.15
0.05 – 0.10
Below 0.05

velocity field shown in Fig. 6 includes the undertow. (Hence, in the breaking zone at some distance from the channel where the beach is a plane slope, the mean velocity will be directed seawards.)

The rip current significantly affects the wave motion. The large variation of the rip current causes a pronounced increase in the wave height which can be seen in Fig. 5b. The wave pattern (in a subdomain) at a time when the circulation cell is fully developed is shown in Fig. 8. It is seen that the effect of the rip current on the wave height counteracts the effect of depth refraction and hence incipient breaking starts locally at the centerline. The rip current also causes a small local bend in the wave crest occurring at the same place. These phenomena can also be seen in a video of the experiment kindly supplied by Hamm.

3.2. A detached breakwater

Comprehensive hydrodynamic measurements around a detached breakwater on a plane beach have recently been reported by Mory and Hamm (1997) and Hamm et al. (1995). The experiments were performed in the same 30 m $\times$ 30 m wave basin as used for the rip current tests. The bed of the basin consists of three sections (see Fig. 9): a 4.4 m wide horizontal section with a water depth of 0.33 m, a plane beach with a slope of 1:50 between the horizontal section and the shoreline, and an emerged plane beach with a slope of 1:20 and cresting at 0.66 m. A half detached breakwater 6.66 m long and 0.87 m wide is placed parallel to the shoreline along a vertical wall. The onshore side of the breakwater is located 9.33 m from the shoreline. An absorbing beach is placed on the offshore side of the breakwater and along the vertical wall opposite to the breakwater. In the experiments, the following four wave conditions were considered: regular, unidirectional waves of normal incidence, wave period of 1.69 s and wave heights of 0.121 m (REG2806) and 0.080 m (REG0107), respectively; irregular, unidirectional waves of normal incidence sampled from a JONSWAP spectrum with peak period of 1.69 s and significant wave height of 0.115 m (UNI3006); and irregular waves as UNI3006, but with directions sampled from a $\cos^2\theta$ directional distribution with mean direction normal to the beach (DIR0407).

In the numerical simulations, the physical wavemaker is replaced by an internal line of generation, and re-reflection from the boundary is avoided by using a 1 m wide sponge layer offshore from the generation line. The absorbing beach on the offshore side of the breakwater and along the vertical wall opposite to the breakwater was modelled using a porosity layer. Bed friction was modelled using a friction factor of $f_m = 0.005$. This value was determined by calibration. The grid spacing was 0.05 m, the timestep was 0.03 s and the simulation period was 608.4 s corresponding to 360 wave periods.

Numerical simulations have been performed for the two test cases: REG0107 and DIR0407. The variation of the wave heights and the setup agrees quite well with the

Fig. 16. Circulation cell behind the detached breakwater for the case of irregular, multidirectional waves. Computed time-average of the velocities beneath the surface rollers. (a) Vector plot and (b) contour plot of the speed.

measurements in both cases. The cross-shore variations of the wave height and setup taken at different sections are shown in Figs. 10–13 for the two cases. Note that the data for the setup were not always provided at the same cross-sections as the wave heights. In general, the breaking zone is wider for the case with random waves than for the case with regular waves and the setup is seen to be smoother for the random waves.

In the experiments, a strong circulation cell was observed behind the breakwater. This large eddy is also reproduced by the numerical model for both the regular and irregular case. The computed current field for the case of regular waves (REG0107) is shown in Fig. 14. The vector plot shows results at every 20th grid point. Here, the velocities are the depth-averaged velocities under the roller obtained by averaging over the last 6 wave periods. Detailed measurements of the current field using Laser-Doppler Anemometer (LDA) were performed for the regular, unidirectional case. In the experiment, the velocities were measured at mid-depth in 60 locations behind the breakwater. Additionally, the vertical profiles of the two mean velocity components were measured in selected positions and these data showed that the horizontal components of the velocity were nearly uniform over the water-depth in the region behind the breakwater. The measured velocity field obtained by averaging over 236 wave periods is shown in Fig. 15. It is seen by comparing Fig. 14a and Fig. 15 that the computed eddy structure agrees quite closely with the measured structure with respect to the location of the eddy, the size of the large quiescent area in the center of the eddy, and the maximum speed. A number of state-of-the-art models based on the decoupled approach have been applied to the same example (Péchon et al. (1997) and Péchon and Desitter (1995)) and they all underestimate the size of the quiescent area. For the present results, the main discrepancy is seen in the area outside the lee of the breakwater: The model results show that the strong jet along the wall of the breakwater is only slowly disintegrated and bent towards the shoreline, while in the experiment, the jet is bent very strongly at the tip of the breakwater. This indicates that the current is too strongly convection-dominated in the numerical simulations. It should be noted that the velocity field shown in Fig. 14 also includes the undertow.

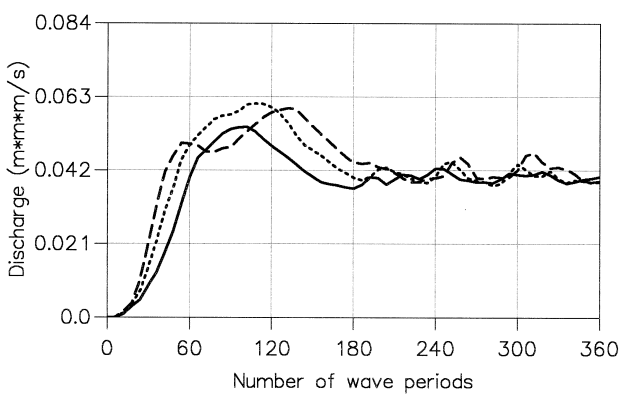

Fig. 17. Time variation of the discharge across three sections extending from the breakwater to the center of the eddy for the case of regular, unidirectional waves. ————, $y = 3$ m, . . . $y = 4$ m; and ---, $y = 5$ m.

Fig. 16 shows the computed current field for the case of directional random waves (DIR0407). In this case, the velocities are obtained by averaging over the last 240 wave periods. Compared to the case with regular waves, the main features of the eddy structure for random waves is that the quiescent area in the center of the eddy and the maximum speed are reduced. These main differences were also observed during the experiments by visualization using tracking of dye clouds and by measurements of the mean current along two lines parallel to the breakwater ($x = 0.32$ m) and the shoreline ($x = 5.60$ m). The current measurements at $x = 0.32$ m showed a reduction in the maximum velocity speed of 30% behind the breakwater. Unfortunately, the measurements were not as extensive as for the regular case and no LDA measurements of the current field were performed.

The time scale for developing the steady eddy pattern in the numerical model is discussed in the following. First, a small eddy with rotation in the eddy core appears near $(x, y) = (3,7)$. When the simulation is continued, a quiescent area in the core of the eddy starts to develop and the center of the eddy is moved behind the breakwater. As an

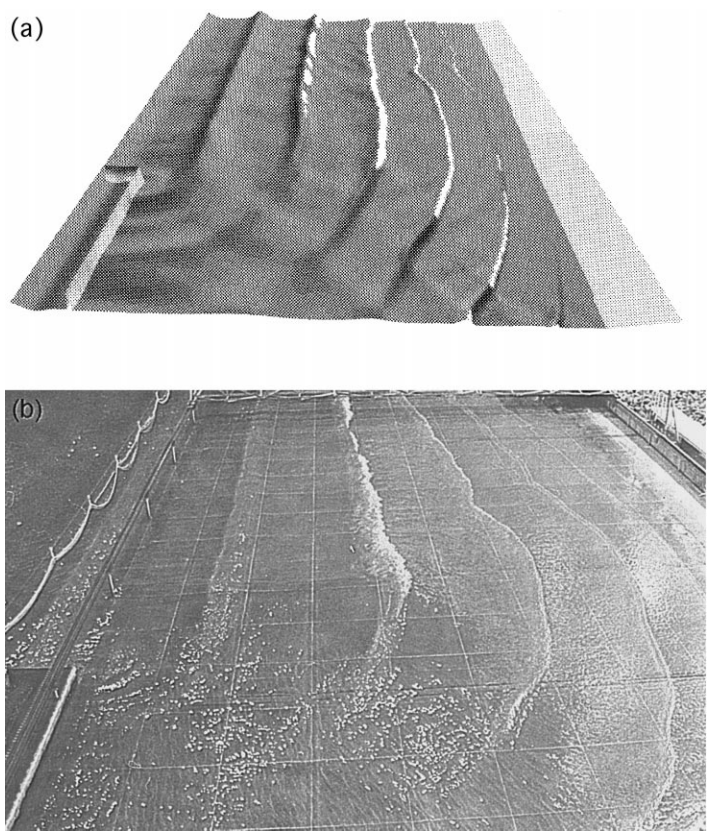

Fig. 18. Instantaneous surface elevation for the case of regular, unidirectional waves. (a) Present model; (b) Photograph by Mory and Hamm (1997).

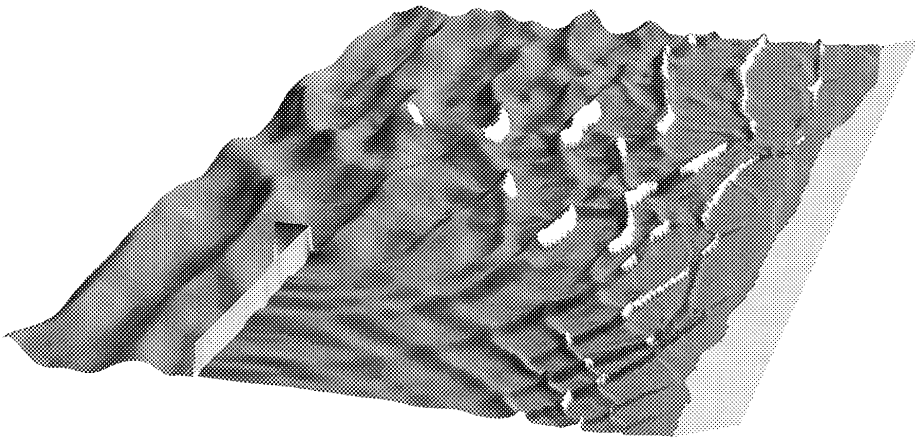

Fig. 19. Instantaneous surface elevation for the case of irregular, multidirectional waves. Present model.

indication of the time scale for the development of the eddy structure, the time variation of the discharge across three sections at $y = 3$, 4 and 5 m from the breakwater to the center of the eddy is shown in Fig. 17. It is seen that a steady state is reached after approximatly 180 wave periods (304.2 s). Estimated from the measurements the discharge at $y = 3$ m is 0.042 m^3/s, and the calculated steady state result is seen to be very close to this value.

The numerical results also show an eddy structure along the lateral wall opposite to the breakwater, and along the shoreline a number of small eddies generate rip currents. The generation of the small eddies is initialized by the oscillation in the wave height caused by the diffraction of the waves around the breakwater. The tracking of dye clouds also showed a return current along the lateral wall and indicated the existence of a rip current. However, more detailed data are needed for a quantitative comparison of the rip currents.

Snapshots of the surface elevation for REG0107 and DIR0407 are shown in Figs. 18 and 19, respectively. For the case of regular waves, a forward bend in the wave fronts can be seen near the breakwater. This phenomenon is caused by the strong following current with a maximum Froude number of approximately 0.2. A similar feature was observed in the experiments as seen from the photograph in Fig. 18b.

4. Summary and conclusion

Wave-driven nearshore circulation has been studied using a coupled approach provided by a Boussinesq-type model. The model, which was presented in Part I of this work, resolves the primary wave motion as well as long waves and wave-induced currents. Wave breaking is included using a surface roller concept and the shoreline is treated by a run-up condition.

The paper details some aspects relevant to the case of two horizontal dimensions including the geometrical determination of surface rollers. In general, both the initial and the final stage of the breaking process can be represented within the same instantaneous roller of a breaking wave. Hence, to capture this phenomenon, the angle determining the roller toe points must be allowed to vary along the wave front.

Application to two examples of wave-generated nearshore circulation currents shows good agreement with laboratory measurements both with respect to the variation of the wave heights and setup and the resulting wave-induced current patterns. The simulations show details of the wave–current interaction which in the traditional decoupled approach of wave and current computations can be obtained only by iterative model executions. Furthermore, the present method has the potential to simulate much more complicated phenomena such as low frequency motions, which are either gravity dominated (e.g., edge waves) or vorticity dominated (shear waves).

The present state of two-dimensional surf zone modelling based on Boussinesq type equations is far less mature than the cross-shore motions reported in Parts I and II of this work. However, the results obtained so far are promising, and this type of model is expected to be a useful tool for the study of many coastal phenomena in the future.

Acknowledgements

Many thanks are due to Luc Hamm who kindly provided experimental data for comparisons. This work was financed by the Danish National Research Foundation. Their financial support is greatly appreciated.

References

Abbott, M.B., Larsen, J., Madsen, P.A., Tao, J., 1983. Simulation of wave breaking and runup. In: Seminar on Hydrodynamics of Waves in Coastal Areas, Vol. 7. Arranged by IAHR in connection with the 20th Congress, Moscow, pp. 146–149.

Basco, D.R., 1982. Surfzone currents. Miscellaneous Report No. 82-7. U.S.A.E., Coastal Engineering Research Center, September 1982.

Basco, D.R., 1983. Surfzone currents. Coastal Eng. 7, 331–355.

Battjes, J.A., Sobey, R.J., Stive, M.J.F., 1990. Nearshore circulation. Sea Ocean Eng. Sci. A 9, 467–493.

Chen, Q., Madsen, P.A., Sørensen, O.R., Basco, D.R., 1996. Boussinesq equations with improved Doppler shift and dispersion for wave/current interaction. Proc. 25th Int. Conf. Coastal Eng., Orlando, USA, 1996. ASCE, New York, 1997, pp. 1060–1073.

Deigaard, R., 1989. Mathematical modelling of waves in the surf zone. Prog. Report 69, ISVA, Danish Technical University, Lyngby.

Ebersole, B.A., Dalrymple, R.A., 1979. A numerical model for nearshore circulation including convective accelerations and lateral mixing. Ocean Engineering, Rep. 21, University of Delaware, Delaware.

Hamm, L., 1992a. Directional nearshore wave propagation over a rip channel: an experiment. Proc. 23rd Int. Conf. Coastal Eng., Venice, Italy, 1992. ASCE, New York, 1993, pp. 226–239.

Hamm, L., 1992b. Random wave propagation in the nearshore zone: experiments in a directional wave basin. Internal report, MAST-G6M, SOGREAH.

Hamm, L., Mory, M., Peronnard, C., 1995. Hydrodynamic measurements around a detached breakwater in a 3D wave basin. Internal report, MAST-G8M, SOGREAH.

Kabiling, M.B., Sato, S., 1993. Two-dimensional nonlinear dispersive wave-current and three-dimensional beach deformation model. Coastal Eng. Jpn. 36, 196–212.

Karambas, Th., Kretenitis, Y., Koutitas, C., 1990. A numerical solution of Boussinesq equations in the inshore zone. Hydro Soft 3 (1), 34–37.

Kirby, J.T., Dalrymple, R.A., 1984. Surfzone currents, by D.R. Basco—Discussion. Coastal Eng. 8, 387–392.

Leonard, B.P., 1991. The ULTIMATE conservative difference scheme applied to unsteady one-dimensional advection. Comput. Meth. Appl. Mechanics Eng. 88, 17–74.

LeVeque, R.J., 1990. Numerical methods for conservation laws, Lectures in Mathematics ETH, Zürich, Birkhäuser.

Madsen, P.A., Schäffer, H.A., 1998. Higher order Boussinesq-type equations for surface gravity waves—derivation and analysis. Accepted for publication in Philos. Trans. R. Soc.

Madsen, P.A., Sørensen, O.R., 1992. A new form of the Boussinesq equations with improved linear dispersion characteristics: Part 2. A slowly varying bathymetry. Coastal Eng. 18, 183–204.

Madsen, P.A., Murray, R., Sørensen, O.R., 1991. A new form of the Boussinesq equations with improved linear dispersion characteristics. Part 1. Coastal Eng. 15, 371–388.

Madsen, P.A., Sørensen, O.R., Schäffer, H.A., 1994. Time domain modelling of wave breaking, runup and surf beats. Proc. 24th Int. Conf. Coastal Eng., Kobe, Japan, 1994. ASCE, New York, 1995, pp. 399–411.

Madsen, P.A., Sørensen, O.R., Schäffer, H.A., 1997a. Surf zone dynamics simulated by a Boussinesq type model. Part I. Model description and cross-shore motion of regular waves. Coastal Eng. 32, 255–288.

Madsen, P.A., Sørensen, O.R., Schäffer, H.A., 1997b. Surf zone dynamics simulated by a Boussinesq type model. Part II. Surf beat and swash oscillations for wave groups and irregular waves. Coastal Eng. 32, 289–320.

Mory, M., Hamm, L., 1997. Wave height, setup and currents around a detached breakwater submitted to regular or random wave forcing. Coastal Eng. 31, 77–96.

Péchon, P., Desitter, A., 1995. Comparison of computed three-dimensional wave-driven currents with measurements. Proc. Coastal Dynamics 95, Gdansk, pp. 513–520.

Péchon, P., Rivero, F., Johnson, H., Chesher, T., O'Conner, B., Tanguy, J.-M., Karambas, T., Mory, M., Hamm, L., 1997. Intercomparison of wave-driven current models. Coastal Eng. 31, 199–215.

Prüser, H.-H., 1991. Zur mathematischen Modellierung der Interaktion von Seegang und Strömung im flachen Wasser. Report No. 31, Institut für Strömungsmechanik und elektronisches Rechnen im Bauwesen, Universität Hannover.

Schäffer, H.A., Deigaard, R., Madsen, P.A., 1992. A two-dimensional surf zone model based on the Boussinesq equations. Proc. 23rd Int. Conf. Coastal Eng., Venice Italy, 1992. ASCE, New York, 1993, pp. 576–589.

Schäffer, H.A., Madsen, P.A., Deigaard, R., 1993. A Boussinesq model for waves breaking in shallow water. Coastal Eng. 20, 185–202.

Sørensen, O.R., Schäffer, H.A., Madsen, P.A., Deigaard, R., 1994. Wave breaking and induced nearshore circulations. Proc. 24th Int. Conf. Coastal Eng., Kobe, Japan, 1994. ASCE, New York, 1995, pp. 2583–2591.

Vreugdenhil, C.B., 1980. A method of computation for unsteady wave-driven coastal currents. Rep. No. 1174, Part 1, Delft Hydraulics, Aug 1980, the Netherlands.

Vreugdenhil, C.B., Koren, B., 1993. Numerical methods for advection diffusion problems. Notes on Numerical Fluid Mechanics, Vol. 45, Vieweg.

Watanabe, A., Dibajnia, M., 1988. A numerical model of wave deformation in surf zone, Proc. 21st Int. Conf. Coastal Eng. ASCE, New York, 1989, pp. 578–587.

Wu, C.S., Liu, P.L.F., 1982. Finite element modelling of breaking wave-induced nearshore current. In: Kawai, T. (Ed.), Finite Element Flow Analysis, pp. 579–586.

Yoon, S.B., Liu, P.L.-F., 1989. Interactions of currents and weakly nonlinear water waves in shallow water. J. Fluid Mechanics 205, 397–419.